An Optimal Path for an Autonomous Vehicle: A nonparametric approach

Ronaldo Dias*, Nancy L. Garcia, Adriano Z. Zambom
Universidade Estadual de Campinas (UNICAMP)

June 26, 2007

Abstract

The objective of this study is to find the best trajectory for an autonomous vehicle which has to move from point A to point B in the minimum distance possible while avoiding all fixed obstacles between these points. Moreover, we assume that there is a safe distance r to be kept between the vehicle and the obstacles at all times. Also, the maneuverability of the vehicle is not easy, that is it cannot make abrupt turns and the trajectory has to follow a smooth curve. Obviously, if there are no obstacles, the best route is a straight line between A and B. In this work we propose a nonparametric method of finding the best path. If there is measurement error, a consistent stochastic estimator is proposed in the sense that as the number of observations increase the stochastic trajectory converges to the deterministic one.

Index terms: autonomous vehicle, B-splines, optimization, consistent estimator, confidence ellipses.

*Corresponding author: Departamento de Estatística, IMECC/UNICAMP – Caixa Postal 6065, 13.081-970 - Campinas, SP - BRAZIL, e-mail addresses: dias@ime.unicamp.br, nancy@ime.unicamp.br, adrzzz@yahoo.com

1 Introduction

From the DARPA Grand Challenge (http://www.darpa.mil/grandchallenge) we take the following definition: "An autonomous ground vehicle is a vehicle that navigates and drives entirely on its own with no human driver and no remote control. Through the use of various sensors and positioning systems, the vehicle determines all the characteristics of its environment required to enable it to carry out the task it has been assigned."

In this work, we are assuming that the autonomous vehicle has to move from point A to point B in the minimum distance possible while avoiding all fixed obstacles between these points. Moreover, we assume that there is a safe distance r to be kept between the vehicle and the obstacles at all times. Also, we assume that the maneuvering of the vehicle is not easy, that is it cannot make abrupt turns and the trajectory has to follow a smooth curve. Obviously, if there are no obstacles, the best route is a straight line between A and B.

The proposed procedure considers only obstacle that cannot be transposed even in low velocities. Moreover, the penalization approach takes into account only the feasible trajectories thus saving computer resources and time.

Without loss of generality we can consider $A = (0, 0)$ and $B = (b, 0)$ (if not, a rotation of the plane will accomplish the change). For a function $f : [0, b] \to \mathbb{R}$ such that $f(0) = 0$ and $f(b) = 0$, then

$$\text{Graf}\,(f) \;=\; \{(x, y); x \in [0, b] \text{ and } y = f(x)\}$$

represents a trajectory in the plane from point A to point B. To be precise on what we called a smooth trajectory, consider only functions f belonging to the Sobolev space $\mathcal{H}_2^2 := \{f : f' \text{ abs. continuous and } \int (f'')^2 < \infty\}$. This is an infinite-dimensional space, however one may assume that f can be well approximated by a function belonging to a finite dimensional space $\mathcal{H}_K$ which is spanned by K (fixed) basis functions, such as Fourier expansion, wavelets, B-splines, natural splines. See, for example, Silverman (1986), Kooperberg and Stone (1991), Vidakovic (1999), Dias (1998) and Dias (2000). Although this fact might lead one to think that the non-parametric problem becomes a parametric problem, one notices that the number of parameters can be as large as the number of observations, and there may be difficulties in estimating the density. Moreover, if the number of observations is large, the system of equations for exact solution is too expensive to solve. This is an inheritance from the approximation theory of functions.

In this paper, we will analyze the problem under two different scenarios: deterministic and stochastic one. In Section 2 the deterministic case is analyst where we will assume that the vehicle has perfect vision and can find the obstacles without error. In this case, the path planning is obtained by solving a penalized optimization problem. In Section 3 we consider that each obstacle is read with some measurement error and a stochastic solution is found. In the case of multiple independent readings the stochastic solution converges to the solution of the deterministic case. Moreover, in Section 4 we consider briefly the case where the vehicle cannot see the whole space. The partial vision is important not only *per se* but because it allows that the vehicle follows a trajectory that cannot be represented by the graph of a function. In this case, the trajectory is constructed piecewisely using the same algorithm. Similar ideas were used in practice during the 2005 DARPA Challenge by Caltech Team, see Cremean et al. (2006).

2 An optimization problem

Assume first that we have L obstacles, with coordinates $\xi_i = (w_i, v_i), \quad i = 1, \ldots, L$. The goal is to find a smooth function belonging to $\mathcal{H}_2^2$ satisfying:

1. The trajectory has to go through the points $A = (0, 0)$ and $B = (b, 0)$, i.e. $f(0) = 0$ and $f(b) = 0$.
2. The distance between any point of Graf (f) and obstacle field $N := \{\xi_1, \ldots, \xi_L\}$ has to be at least r, that is $d(f, \xi_i) \geq r$, for all $i = 1, \ldots, L$ where $d(.,.)$ is the Euclidean distance.
3. The function f minimizes the trajectory in the sense that the length of Graf (f) is minimum.

For any f differentiable, the length of Graf (f) is given by

$$\int_0^b \sqrt{(1 + f'(t)^2)}dt. \tag{2.1}$$

Therefore, we want to find $f \in \mathcal{H}_2^2$ which minimizes

$$Q_r(f) = \int_0^b \sqrt{(1 + f'(t)^2)}dt \tag{2.2}$$

constrained to $d(f, \xi_i) \geq r$, $i = 1, \ldots, L$, $f(0) = 0$ and $f(b) = 0$.

Notice that the constrained minimization problem can be viewed as a penalized problem where the penalty is 0 or ∞ according to $d(f, \xi_i) \geq r$ or not. That is, we want a solution of

$$\min_{f \in \mathcal{H}_2^2} \int_0^b \sqrt{(1 + f'(t))^2} dt + J^*(f) \tag{2.3}$$

where

$$J^*(f) = \begin{cases} 0, & \text{if } d(f, \xi_i) \geq r, \quad i = 1, ..., L \\ \infty, & \text{if } d(f, \xi_i) < r, \quad i = 1, ..., L. \end{cases} \tag{2.4}$$

However, there is no smooth solution for this kind of penalization. To overcome this problem, first we approximate the penalization by the smooth functional

$$J_{\psi,\alpha,n}(f) = \psi \Phi(Z_\alpha + \sqrt{n}(r - d(f, N))) \tag{2.5}$$

where Φ is the cumulative standard Gaussian distribution, Z_α is its αth percentile and (ψ, α, n) are tuning parameters. This penalization is convenient since it follows that $J_{\psi,\alpha,n}(f) \to J^*(f)$ when $\psi \to \infty$, $\alpha \to 0$ and $n \to \infty$. In Section 2.1 we explain the roles of the tuning parameters.

Second, we will fix K and a sequence $\mathbf{t} = (t_1, \ldots, t_{K-2})$ and consider f belonging to the space $\mathcal{H}_K$ spanned by B-splines with interior knot sequence $\mathbf{t}$. That is,

$$f(x) \; = \; f_{\boldsymbol{\theta}}(x) \; = \; \sum_{j=1}^{K} \theta_j B_j(x) \tag{2.6}$$

where B_j are the well-known cubic B-spline basis (order 4) and $\boldsymbol{\theta} = (\theta_1, \ldots, \theta_K)$ is a vector of unknown coefficients.

Figure 2.1 presents 6 B-splines functions for equally spaced knots in the intervals $[0, 10]$. From the picture we can see some of the most useful computational properties presented by B-splines. They are splines which have smallest possible support. In other words, B-splines are zero in a large set. Furthermore, a stable evaluation of B-splines with the aid of a recurrence relation is possible. For details, see de Boor (1978).

Therefore, we want to find $f_{\boldsymbol{\theta}} \in \mathcal{H}_k$, or equivalently $\boldsymbol{\theta} = (\theta_1, \ldots, \theta_K) \in \mathbb{R}^K$ which minimizes

$$Q_{\alpha,\psi,r,n}(\boldsymbol{\theta}) = \int_0^b \left(1 + (\sum_{j=1}^{K} \theta_j B_j'(t))^2 \right)^{1/2} dt + \psi \, \Phi \left(Z_\alpha + \sqrt{n}(r - d(\sum_{j=1}^{K} \theta_j B_j(\cdot), N)) \right), \tag{2.7}$$

subject to $f_{\boldsymbol{\theta}}(0) = 0, f_{\boldsymbol{\theta}}(b) = 0$.

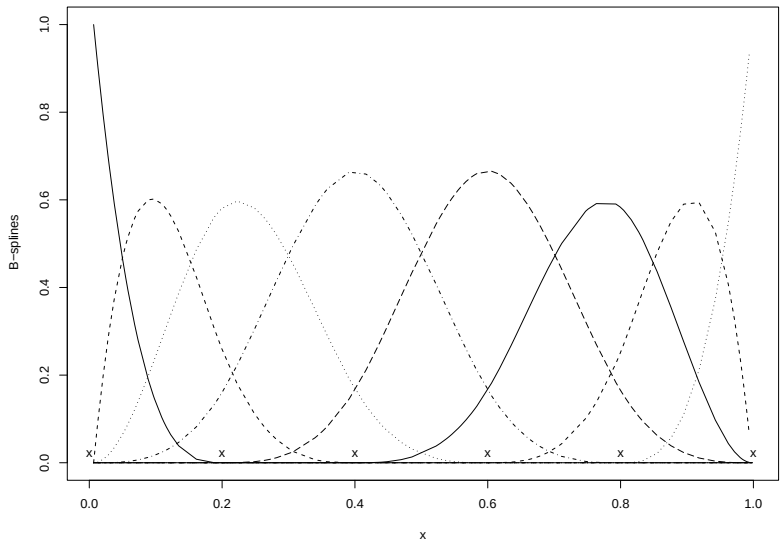

Figure 2.1: Basis Functions with 6 knots placed at $\mathbf{t} = (0.0, 0.2, 0.4, 0.6, 0.8, 1.0)$

2.1 The tuning parameters

Notice that the functionals J^* and $J_{\psi,\alpha,n}$ depend on the function f only through its distance to the obstacle field ($d(f, N)$), thus we can think of them as real-valued functions. The function $J_{\psi,\alpha,n}$ is a continuous analog of J^*. The roles of the tuning parameters (ψ, α, n) are $\psi\alpha = J_{\psi,\alpha,n}(r)$, $\psi = \max_{x\geq 0} J_{\psi,\alpha,n}(x)$ and n controls the steepness of $J_{\psi,\alpha,n}$ at the point r. They should be chosen in such way that, when the trajectory tries to violate the restriction that the distance between the vehicle and the obstacles have to be bigger than r at all times, the penalization is so much bigger than the gain in the distance that this trajectory cannot occur. Figure 2.2 shows the effect of the tuning parameter n on the penalty $J_{\psi,\alpha,n}(f)$, for a better visualization we fixed $\psi\alpha = 30$. However, for computation and numerical examples we will use $\alpha.\psi = 0.05$.

Tables 2.1, 2.2 and 2.3 present some simulation results for a set of 3 obstacle fields given by Figures 2.3, 2.4 and 2.5. These fields present increasing degrees of difficulty for the vehicle to find the best trajectory. Notice that as ψ increases (α decreases, recall that $\psi = 0.05/\alpha$) and/or n increases we get closer and closer to the best trajectory until it stabilizes. From these

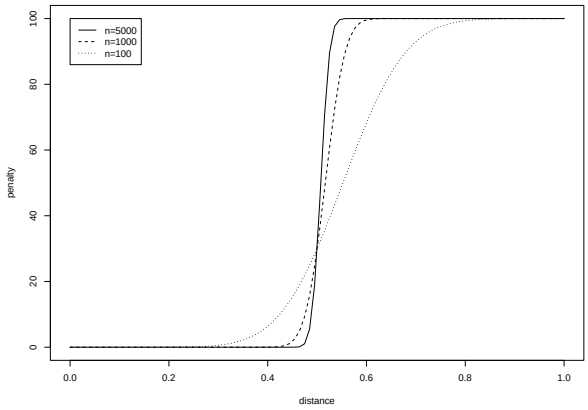

Figure 2.2: Effect of the tuning parameter n on the penalty function $J_{\psi,\alpha,n}(f)$, $\psi = 100$, $\alpha = 0.3$, $r = 0.5$.

α	$3.333 * 10^{-9}$	$3.333 * 10^{-8}$	$3.333 * 10^{-7}$	$3.333 * 10^{-6}$
$n * 10^{-3}$				
.5	15.29637	15.29671	15.29717	15.29781
1	15.29076	15.29179	15.29303	15.29454
5	15.28292	15.28317	15.28353	15.28404
10	15.28216	15.28223	15.28233	15.28249
20	15.28202	15.28202	15.28204	15.28206
40	15.28202	15.28201	15.28201	15.28201
50	15.28202	15.28201	15.28201	15.28201
150	15.28202	15.28201	15.28201	15.28201
1500	15.28202	15.28201	15.28201	15.28201
15000	15.28201	15.28201	15.28201	15.28201

Table 2.1: $\min_{\boldsymbol{\theta}} Q_{Z_\alpha,\psi,r,n}(\boldsymbol{\theta})$ for Obstacle Field 1 presented in Figure 2.3. The length of the chosen trajectory for $n = 500$ is 15.29503 and for all other values of n, it is 15.28201.

α	$1.666 * 10^{-9}$	$1.666 * 10^{-8}$	$1.666 * 10^{-7}$	$1.666 * 10^{-6}$
$n * 10^{-3}$				
.5	30.2067	30.54674	30.2067	30.2067
1	30.20574	30.2067	30.2067	30.2067
5	30.19141	30.19238	30.19354	30.19495
10	30.18695	30.1876	30.18842	30.18947
20	30.18436	30.18467	30.18510	30.18568
40	30.18333	30.18343	30.18356	30.18377
50	30.18321	30.18326	30.18335	30.18348
300	30.18308	30.18308	30.18308	30.18308
3000	30.18308	30.18308	30.18308	30.18308
30000	30.18308	30.18308	30.18308	30.18308

Table 2.2: $\min_{\boldsymbol{\theta}} Q_{Z_\alpha,\psi,r,n}(\boldsymbol{\theta})$ for Obstacle Field 2 presented in Figure 2.4. The length of the chosen trajectory for $n = 500, 1000$ is 30.2067 and for all other values of n, it is 30.18308.

α	$8.333 * 10^{-10}$	$8.333 * 10^{-9}$	$8.333 * 10^{-8}$	$8.333 * 10^{-7}$
$n * 10^{-3}$				
.5	60.03327	60.03329	60.03332	60.03338
1	60.03322	60.03322	60.03332	60.03332
5	60.03322	60.03322	60.03332	60.03332
10	60.03322	60.03322	60.03332	60.03332
20	60.03322	60.03322	60.03332	60.03332
40	60.03322	60.03322	60.03332	60.03332
50	60.03322	60.03322	60.03332	60.03332
600	60.03322	60.03322	60.03322	60.03332
6000	60.02502	60.02542	60.02594	60.02663
60000	60.0231	60.0231	60.0231	60.02311

Table 2.3: $\min_{\boldsymbol{\theta}} Q_{Z_\alpha,\psi,r,n}(\boldsymbol{\theta})$ for Obstacle Field 3 presented in Figure 2.5. The length of the chosen trajectory for $n \leq 600 * 10^3$ is 60.03322 and for all other values of n, it is 60.0231.

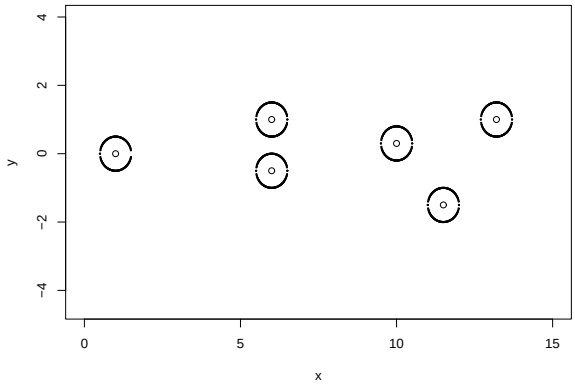

Figure 2.3: Obstacle Field 1

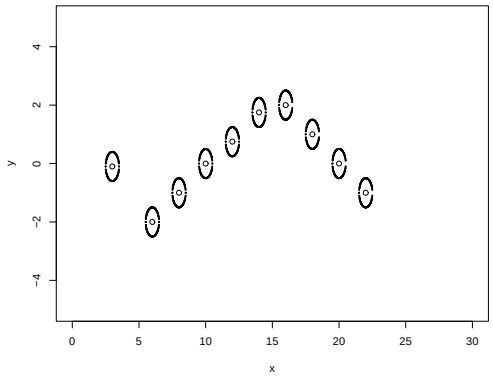

Figure 2.4: Obstacle Field 2

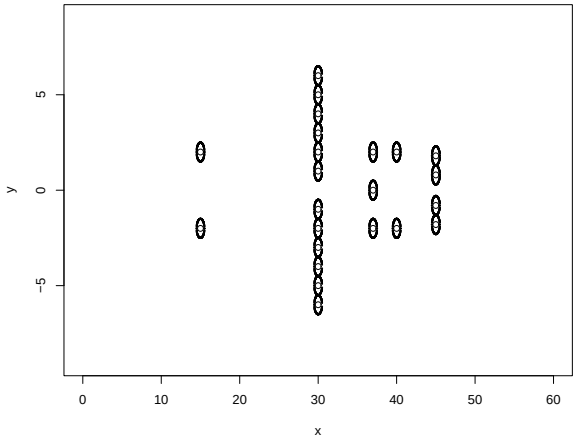

Figure 2.5: Obstacle Field 3

simulated results, we choose $\psi = 10^6 b$, $\alpha = 0.05/\psi$ e $n = 10^6 b$.

How many knots? In fact, in approximation theory, one of the most challenging problem is how to select the dimension of the approximant space. A similar problem is encountered in the field of image processing where the level of resolution needs to be determined appropriately.

Figure 2.6 presents several obstacle fields with different degrees of difficulty for finding a trajectory. These fields were construct to test the strength of the algorithm since the best route is not "easy". We could see that increasing the number of interior knots above 4 did not bring

any improvement. With 3 or 4 interior knots we obtain the "best" possible $f_{\boldsymbol{\theta}}$. If necessary, the choice of the number of knots can be very adaptive, see for example Gu (1993), Antoniadis (1994) De Vore, Petrova and Temlyakov (2003), Bodin, Villemoes and Wahlberg (2000), Kohn, Marron and Yau (2000) and easily implemented.

3 A stochastic problem. Complete Vision

In the previous section, we assumed that the sensors of the vehicle can see the whole field and detect with certainty the placement of the obstacles. This is not realistic, there is always a measurement error involved. In this section, we will suppose that the vehicle can see the whole field (partial vision will be considered in Section 4) but instead of seeing N, it sees:

$$\eta = N + \boldsymbol{\varepsilon}$$

where $\boldsymbol{\varepsilon} = (\varepsilon_1, \ldots, \varepsilon_L)$ is the measurement error. Specifically, we will assume that the vehicle sees a field composed of independent random variables

$$(W_\ell, V_\ell) = (w_\ell, v_\ell) + (\varepsilon_{\ell 1}, \varepsilon_{\ell 2}), \quad \ell = 1, ..., L \tag{3.1}$$

where $(\varepsilon_{\ell 1}, \varepsilon_{\ell 2}) \sim N_2((0,0), \boldsymbol{\Sigma}_i)$, $\ell = 1, \ldots, L$ and independent and $\boldsymbol{\Sigma}_\ell$ is a covariance matrix (that can depend on the obstacle) given by

$$\boldsymbol{\Sigma}_\ell = \begin{pmatrix} \sigma_{\ell,1}^2 & \rho\sigma_{\ell,1}\sigma_{\ell,2} \\ \rho\sigma_{\ell,1}\sigma_{\ell,2} & \sigma_{\ell,2}^2 \end{pmatrix}. \tag{3.2}$$

This scenario incorporates several practical situations, for example large variance for dark spots, increasing variance depending of the distance to the obstacle, etc.

Moreover, we have for each obstacle, n independent readings. Thus, our data is composed of n readings of the obstacle field $\eta_i = \{(W_{1,i}, V_{1,i}), \ldots, (W_{L,i}, V_{L,i})\}$ for $i = 1, \ldots, n$. Denote $\mathbf{W}_\ell = (W_{\ell,1}, \ldots, W_{\ell,n})$ and $\mathbf{V}_\ell = (V_{\ell,1}, \ldots, V_{\ell,n})$, $\ell = 1, \ldots, L$.

For fixed $\gamma \in (0,1)$, the proposed estimator for $f_{\boldsymbol{\theta}}$ is the function

$$f_{\boldsymbol{\theta}^*}^{\gamma}(x) = \sum_{j=1}^{K} \theta_j^* B_j(x) \tag{3.3}$$

a) length = 15.89602

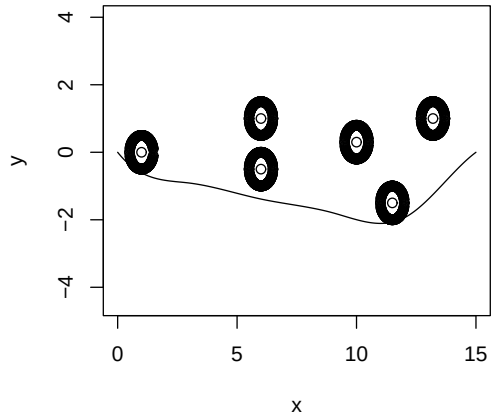

b) length = 15.24145

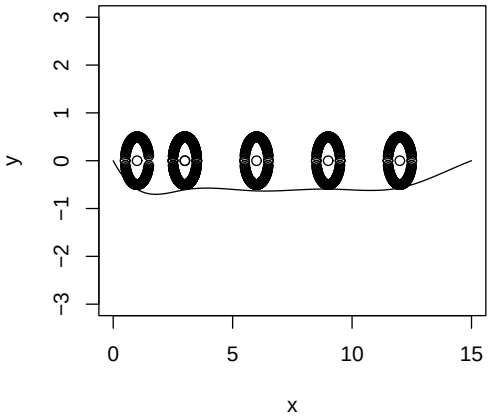

c) length = 15.64931

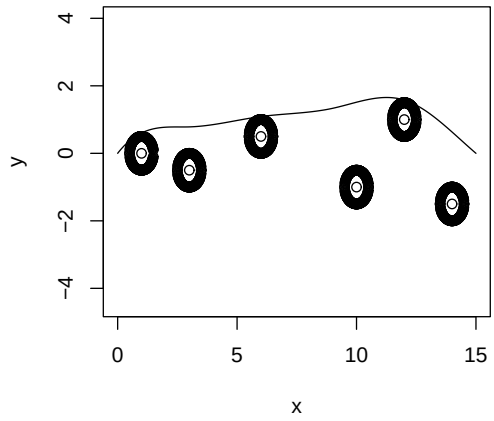

d) length = 15.40389

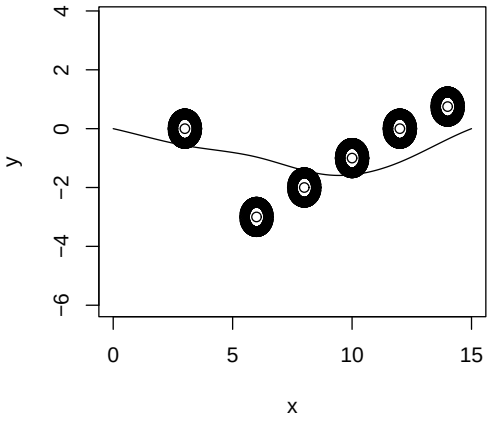

e) length = 15.84148

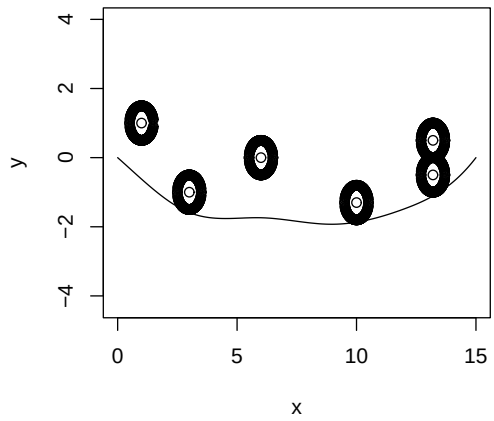

f) length = 15.73737

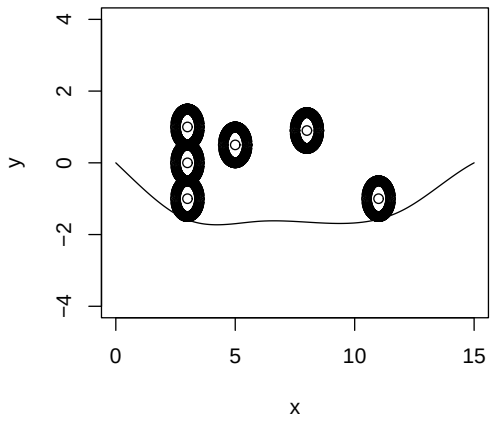

Figure 2.6: Obstacle fields and the estimated "best" trajectory using 4 internal knots

where $\boldsymbol{\theta}^*$ is the solution of the minimization problem

$$\boldsymbol{\theta}^* = \arg\min \int_0^b \left(1 + (\sum_{j=1}^{K} \theta_j B_j'(t))^2\right)^{1/2} dt + \psi\, \Phi\left(Z_\alpha + \sqrt{n}(r - d(\sum_{j=1}^{K} \theta_j B_j(\cdot), \eta^\gamma)\right), \quad (3.4)$$

subject to $f_{\boldsymbol{\theta}}^{\gamma}(0) = 0, f_{\boldsymbol{\theta}}^{\gamma}(b) = 0$ (*cf.* with Equation (2.7)). The set η^γ is defined by

$$\eta^\gamma = \bigcup_{\ell=1}^{L} G_\gamma(\mathbf{W}_\ell, \mathbf{V}_\ell) \quad (3.5)$$

where for each $\ell = 1, \ldots, L$, $G_\gamma(\mathbf{W}_\ell, \mathbf{V}_\ell)$ is a $100(1-\gamma)\%$ *confidence ellipse* based on the n readings for the ℓth obstacle $(\mathbf{W}_\ell, \mathbf{V}_\ell)$ defined as the ellipse formed by the points (x, y) that satisfy the equation

$$((\overline{\mathbf{W}}_\ell, \overline{\mathbf{V}}_\ell) - (x, y))^t \boldsymbol{\Sigma}_\ell^{-1} ((\overline{\mathbf{W}}_\ell, \overline{\mathbf{V}}_\ell) - (x, y)) \leq \chi_2^2(\gamma)$$

where $\overline{\mathbf{W}}_\ell$ and $\overline{\mathbf{V}}_\ell$ are the sample average of the vectors $\mathbf{W}_\ell$ and $\mathbf{V}_\ell$ respectively, $\chi_2^2(\gamma)$ is the 100γ-percentile of the chi-square distribution with 2 degrees of freedom. These ellipses are centered at the sample mean $(\overline{\mathbf{W}}_\ell, \overline{\mathbf{V}}_\ell)$ and have axes $(\chi_2^2(\gamma)\sqrt{\lambda_{\ell,j}} e_{\ell,j}, -\chi_2^2(\gamma)\sqrt{\lambda_{\ell,j}} e_{\ell,j})$, where $\lambda_{\ell,j}$, $j = 1, 2$ are the eigenvalues of $\boldsymbol{\Sigma}_\ell$ and $e_{\ell,j}$ are the corresponding eigenvectors. Here, η^γ can be thought as a fattening of the average obstacle field $\bar{\eta} = \frac{1}{n}(\eta_1 + \ldots + \eta_n)$ to account for the variability due to measurement errors.

Remark If the covariance matrices $\boldsymbol{\Sigma}_\ell$ are unknown, the points (x, y) belonging to the confidence ellipses have to satisfy

$$((\overline{\mathbf{W}}_\ell, \overline{\mathbf{V}}_\ell) - (x, y))^t \mathbf{S}_\ell^{-1} ((\overline{\mathbf{W}}_\ell, \overline{\mathbf{V}}_\ell) - (x, y)) \leq F_{2,n-2}(\gamma)$$

where $\mathbf{S}_\ell$ is the standard sample covariance of the vectors $\mathbf{W}_\ell$ and $\mathbf{V}_\ell$ and $F_{2,n-2}(\gamma)$ is the 100γ-percentile of the F distribution with $(2, n-2)$ degrees of freedom.

Figure 3.1 shows confidence ellipse for a bivariate normal distribution centered at one observation.

3.1 Numerical examples

In this section we present simulations performed with different obstacle fields. For illustration purposes, we exhibit the case where we have one and ten readings for each obstacle.

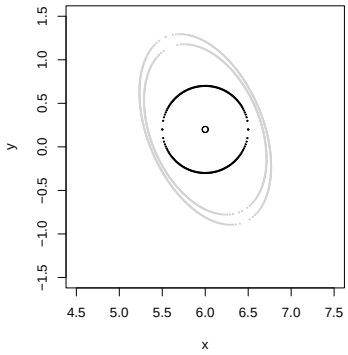

Figure 3.1: Confidence ellipses with $\gamma = 0.05$ and $\gamma = 0.01$ for bivariate normal random variable with $\sigma_1 = 0.1$, $\sigma_2 = 0.2$ e $\rho = -0.8$

In all the plots the black points are the real obstacle, the crosses are mean of the observed obstacles, the confidence ellipses curves are drawn in gray. The solid curve is the curve we would obtain by the procedure described in Section 2 if we had no error. The dashed and dash-point curves are the one obtained by (3.4).

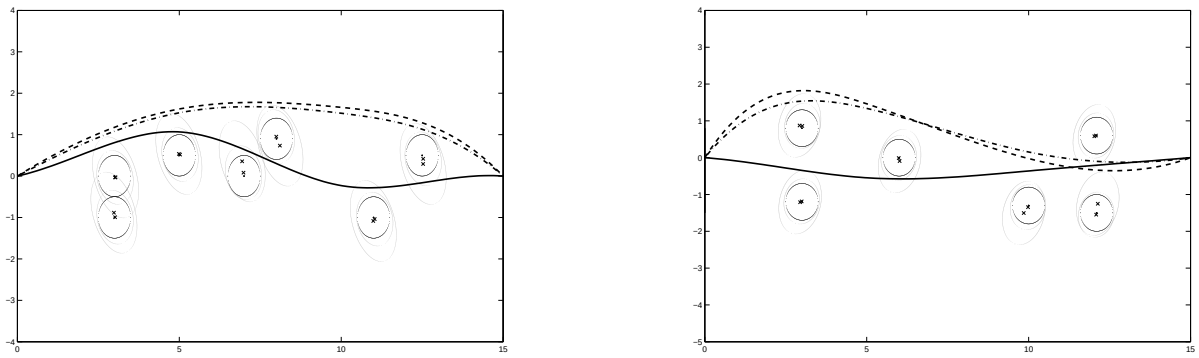

(a) (b)

Figure 3.2: Estimated trajectories for iid case: deterministic trajectory (solid curve), trajectories based on one and ten observations (dashed line, dash-point line). The errors are normally distributed with (a) $\sigma_1 = 0.1$,$\sigma_2 = 0.2$ and $\rho = -0.8$ and (b) $\sigma_1 = 0.07$, $\sigma_2 = 0.15$ and $\rho = 0.6$.

Figures 3.2 and 3.3 show that in the presence of random variability, the paths tend to stay further from the obstacle, but as the number of reading increases it will converge to the

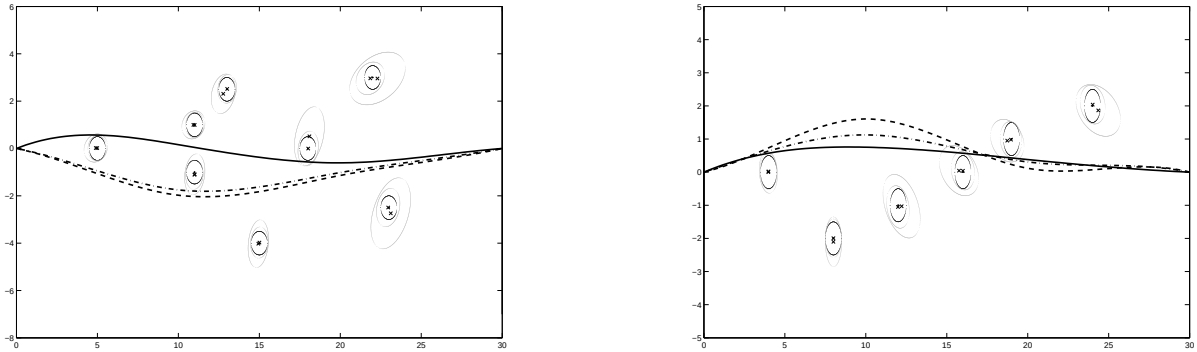

(a) (b)

Figure 3.3: Estimated trajectories for independent case: deterministic trajectory (solid curve), trajectories based on one and ten observations (dashed line, dash-point line). The errors are normally distributed with (a) $\rho = 0.6$, $\sigma_{\ell,1} \sim U(0, (.8/30)W_\ell)$ and $\sigma_{\ell,2} \sim U(0, (.6/30)W_\ell)$, (b) $\rho = -0.7$, $\sigma_{\ell,1} \sim U(0, (.7/30)W_\ell)$ and $\sigma_{\ell,2} \sim U(0, (.5/30)W_\ell)$.

deterministic trajectory.

4 Partial vision

In the previous sections, we assumed that the whole obstacle field can be seen from the starting point and the strategy can be computed before leaving. However, it is more realistic to imagine that the sensors have a finite range R smaller than the total field. In this case, a sequential procedure is necessary. Let us assume that when the vehicle is located at (u, v) it can see up to $S_{u,v} = \{(x, y) : 0 < x - u \leq R\}$. The algorithm to estimate the best trajectory is:

1. Let N_1 be the obstacle field restricted to $S_{(0,0)}$. Let $\hat{f}_1 \in \mathcal{H}_K$ be the minimizer of the cost function
$$\int_0^B \sqrt{1 + f_1'(t)^2}dt + \lambda\Phi(Z_\alpha + \sqrt{n}(r - d(f_1, N_1))) \tag{4.1}$$
where $f_1(0) = 0$, $f_1(b) = 0$.

2. Given the solution $\hat{f}_{i-1}$ at step $i - 1$, let N_i be the obstacle field restricted to $S_{((i-1)R,0)}$. Let $\hat{f}_i \in \mathcal{H}_K$ be the minimizer of
$$\int_0^B \sqrt{1 + f_i'(t)^2}dt + \lambda\Phi(Z_\alpha + \sqrt{n}(r - d(f_i, N_i))), \tag{4.2}$$

subject to $f_i^{(\nu)}((i-1)R) = \hat{f}_{i-1}^{(\nu)}((i-1)R)$, for $\nu = 0, 1, 2$, $f_i(b) = 0$.

This sequential procedure can be interpreted as: the vehicle "thinks" at step i that there is no obstacles after distance R. When it arrives at checkpoints $R, 2R, \ldots$ it restarts the procedure joining smoothly the paths. Another important remark is that, at step i the procedure is not exactly as it was in the beginning because the vehicle will be at a point (iR, y_i), form some y_i not necessarily 0.

Notice that this estimation considers that up to a distance R, the vehicle has perfect vision. The stochastic procedure can be easily implemented in this case.

Figure 4.1 show the simulated results for this case.

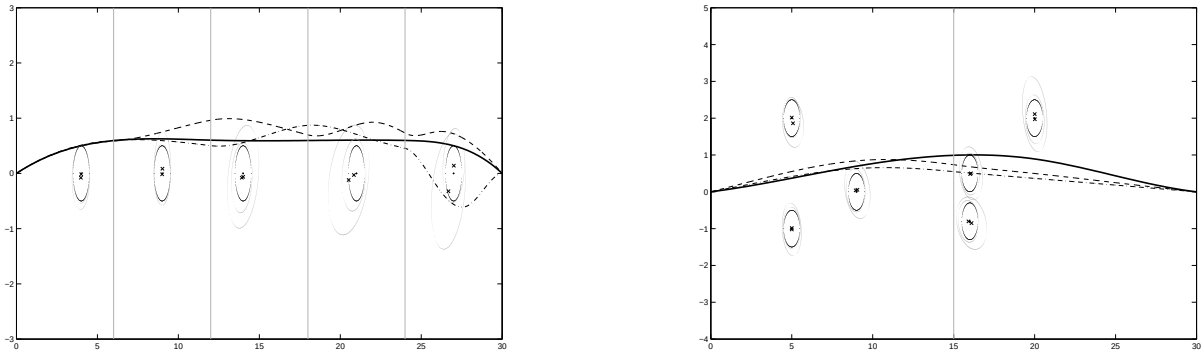

(a) (b)

Figure 4.1: The solid curve is the goal path estimated using (2.7), the dashed and dash-point curves are sequentially estimated reloading stepwisely at the gray vertical lines. The errors are normally distributed with com (a) $\rho = 0.5$, $\sigma_{\ell,1} \sim U(0, (.6/30)W_\ell)$, $\sigma_{\ell,2} \sim U(0, (.4/30)W_\ell)$ and reload at steps of size 6 (b) $\rho = -.6$, $\sigma_{\ell,1} \sim U(0, (.5/30)W_\ell)$, $\sigma_{\ell,2} \sim U(0, (.6/30)W_\ell)$ and reload at steps of size 15.

Figure 4.1(b) raises a very important issue that is to be addressed in a future paper. Since the vehicle only reloads after running the whole R distance, and the path has to be smooth, if there is an obstacle very close to the vehicle when it gets there it will not deviate from it and crashes. To fix this problem, the vehicle should reload at shorter steps and the procedure redone. In this case, a very interesting scenario appears. Assume that the range of vision of the vehicle is R, it reloads after steps of size $R/2^\nu$ and the measurement errors are more precise as the distance between the sensors and the obstacles decrease, how to combine different readings,

for example from point 0, point $R/2^{\nu}$, $R/2^{\nu-1}$, etc?

5 Conclusion

It is important to emphasize that the methodology presented in this paper considers a hypothetical situation which is simpler than the real setting faced by the members of DARPA Great Challenge or any other practical situation. It is necessary to take into account more complex forms of reloading the data (Markovian dependence), allowing obstacles that can be transposed in low velocities, incorporating the race corridor among other real data constraints. The beauty of the penalty approach is its flexibility to allow incorporation of these new factors. However, to face a complex problem it is necessary to dissect it into smaller and simpler pieces. This is the goal of this paper, to begin considering more adaptive obstacle avoidance strategies that can be built efficiently into more sophisticated algorithms.

Acknowledgments It is a pleasure to thank Richard Murray and Timothy Chung for introducing us to this problem and for many fruitful discussions. RD thanks the hospitality and enlightening environment provided by Caltech during his visit. This paper was partially supported by CNPq Grants 301058/2004-0 (RD) and 302279/2004-0 (NG) and FAPESP Grant 2006/02095-5 (AZ).

References

Antoniadis, A. (1994). Wavelet methods for smoothing noisy data, *Wavelets, images, and surface fitting (Chamonix-Mont-Blanc, 1993)*, A K Peters, Wellesley, MA, pp. 21–28.

Bodin, P., Villemoes, L. F. and Wahlberg, B. (2000). Selection of best orthonormal rational basis, *SIAM J. Control Optim.* **38**(4): 995–1032 (electronic).

Cremean, L. B., Foote, T. B., Gillula, J. H., Hines, G. H., Kogan, D., Kriechbaum, K. L., Lamb, J. C., Leibs, J., Lindzey, L., Rasmussen, C. E., Stewart, A. D., Burdick, J. W. and Murray, R. M. (2006). Alice: An information-rich autonomous vehicle for high-speed desert navigation, *Journal of Field Robotics* **23**(9): 777–810.

de Boor, C. (1978). *A Practical Guide to Splines*, Springer Verlag, New York.

De Vore, R., Petrova, G. and Temlyakov, V. (2003). Best basis selection for approximation in L_p, *Found. Comput. Math.* **3**(2): 161–185.

Dias, R. (1998). Density estimation via hybrid splines, *Journal of Statistical Computation and Simulation* **60**: 277–294.

Dias, R. (2000). A note on density estimation using a proxy of the Kullback-Leibler distance, *Brazilian Journal of Probability and Statistics* **13**(2): 181–192.

Gu, C. (1993). Smoothing spline density estimation: A dimensionless automatic algorithm, *J. of the Amer. Stat'l. Assn.* **88**: 495–504.

Kohn, R., Marron, J. S. and Yau, P. (2000). Wavelet estimation using Bayesian basis selection and basis averaging, *Statist. Sinica* **10**(1): 109–128.

Kooperberg, C. and Stone, C. J. (1991). A study of logspline density estimation, *Computational Statistics and Data Analyis* **12**: 327–347.

Silverman, B. W. (1986). *Density Estimation for Statistics and Data Analysis*, Chapman and Hall (London).

Vidakovic, B. (1999). *Statistical modeling by wavelets*, Wiley Series in Probability and Statistics: Applied Probability and Statistics, John Wiley & Sons Inc., New York. A Wiley-Interscience Publication.